Available online at www.sciencedirect.com
ScienceDirect
Journal of the European Ceramic Society 27 (2007) 1187–1192
www.elsevier.com/locate/jeurceramsoc

Elaboration and ionic conduction of apatite-type lanthanum silicates doped with Ba, $La_{10-x}Ba_x(SiO_4)_6O_{3-x/2}$ with $x = 0.25$–2

Adrien Vincent [a], Sophie Beaudet Savignat [a,*], François Gervais [b]

[a] *CEA Le Ripault, Département Matériaux, BP 16, 37260 Monts, France*
[b] *UMR 6157 CNRS-CEA, LEMA, Université François Rabelais, Parc de Grandmont 37000 Tours, France*

Available online 30 June 2006

Abstract

The main task in SOFC research is the reduction of the working temperature down to the range 700–800 °C. Apatite ceramics are interesting alternative SOFC electrolytes because of their open structure including tunnels for the diffusion of oxide ions and their good chemical stability. This study reports the influence of barium doping on the microstructural and electrochemical properties of the apatite phase $La_{10-x}Ba_x(SiO_4)_6O_{3-x/2}$ with $x = 0.25$–2. This doping range allows theoretical stoichiometric and overcharged apatite (more than two oxide ions in the tunnel). X-ray diffraction results on fired pellets show total insertion of the barium in the apatite lattice with a linear increase of the lattice parameters following the barium rate. Ionic conductivities are measured under air by impedance spectroscopy between 400 and 900 °C. The results are compared with apatite phases doped with calcium and strontium on the La site.

Keywords: Fuel cells; Powders-solid state reaction; Microstructure-final; Ionic conductivity; Apatite

1. Introduction

The first generation of SOFCs (solid oxide fuel cells) is operated at 1000 °C to insure a sufficient ionic conductivity of their yttria doped zirconia electrolyte. One of the main tasks in SOFCs research is the reduction of the working temperature. A 700 °C working temperature would indeed increase the materials life time and allow the use of cheaper interconnect materials. However, the yttria doped zirconia electrolyte is not a sufficient electrolyte ionic conductor at 700 °C. It becomes therefore essential to develop new electrolyte materials to allow a real evolution of SOFCs technology. One of the best candidates is a ceramic with the apatite structure.[1–7] This structure, with the general formula $(A_6A_4)(MO_4)_6O_2$ with A = Alc, AE, RE, ... and M = Si, Ge, Ga, ...[8], is well known for its great chemical and physical stability. It consists (see Fig. 1) of isolated and covalent silicate tetrahedra which form the "rigid" part of the structure.[9,10] The A_6 cations are located in a seven coordinate site (named 6h) and form a tunnel along the "*c*" axis. The A_4 cations are located in a nine coordinate site (named 4f) between each ionic plane of the structure. The O (2a) anions located in the tunnel formed by A_6 cations and are responsible for the good ionic conductivity of this structure. In this paper we report our work on a range of oxyapatite compositions with Ba doping $La_{10-x}Ba_x(SiO_4)_6O_{3-x/2}$ $x = 0.25$–2, to complete previous works.[11,12] As the existence of the oxyapatite $La_{10}(SiO_4)_6O_3$ is still a subject for discussion, the $La_{9.33}(SiO_4)_6O_2$ composition will be our reference. Previous results[13] report conductivities of respectively, (8.8 and 7.8) $\times 10^{-3}$ S/cm at 700 °C for the compositions $La_9Sr_1Si_6O_{26.5}$ and $La_9Ca_1Si_6O_{26.5}$. Barium doping is in the continuation of these compositions.

2. Experimental

The starting materials were high purity La_2O_3 (Rhodia 99.99%), SiO_2 (Cerac 99.99%) and $BaCO_3$ (Cerac 99.9%). The La_2O_3 and SiO_2 powders were precalcinated at 1100 °C for dehydration. The powders were weighed in the appropriate ratio to elaborate the compounds $La_{10-x}Ba_x(SiO_4)_6O_{3-x/2}$ $(0.25 \leq x \leq 2)$ and $La_{9.33}(SiO_4)_6O_2$ and ball milled in plastic vessels during 24 h before a dry grinding. The powders were calcinated in air at 1500 °C and ground by attrition. Pellets were prepared by uniaxial pressing at 150 MPa and fired under air between 1575 and 1625 °C for 30 min. Phase purity was exam-

* Corresponding author. Tel.: +33 247 344 852; fax: +33 247 345 183.
E-mail address: sophie.beaudet-savignat@cea.fr (S.B. Savignat).

0955-2219/$ – see front matter © 2006 Elsevier Ltd. All rights reserved.
doi:10.1016/j.jeurceramsoc.2006.05.090

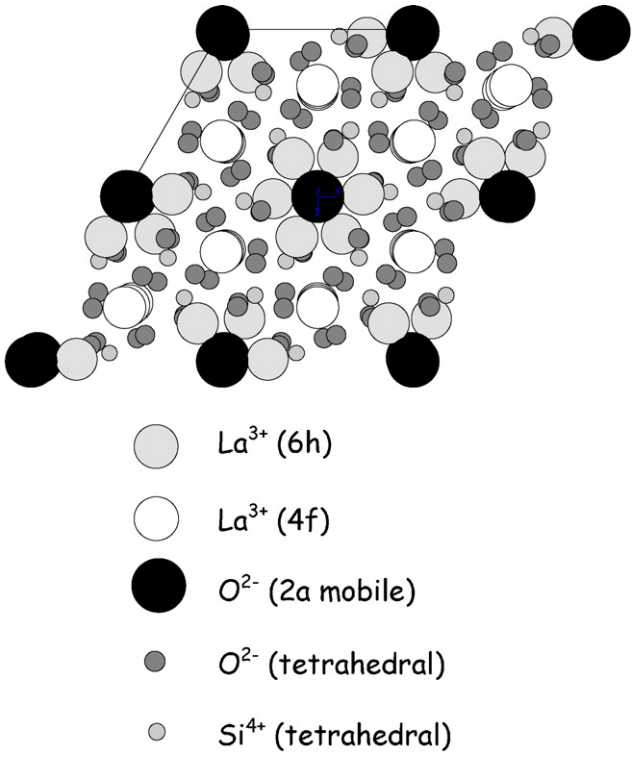

Fig. 1. Apatite structure.

ined on pellets using X-ray diffraction (Cu $K\alpha_1$). X-ray patterns were analyzed by Kdif[14] and Jana 2000[15] softwares to calculate the cell parameters and evaluate phase purity. Microstructure was controlled by scanning electron microscopy on fractured pellets and densities were evaluated by the Archimede method. Dilatometric experiments were carried out in air (Setaram dilatometer TMA92) on uniaxial pressed pellets to study the sintering behavior. AC impedance spectroscopy was carried out in air on dense pellets ($d > 95\%$ of the theoretical) between 400 and 900 °C. Pt electrodes were deposited on both sides of the pellets by PVD under argon plasma. The measurements were collected at 100 mV and between 1.10^6 and 0.1 Hz using Zplot[16] software. Data were analyzed using Zview[17] software. As it was difficult to separate grain and bulk boundary contributions on the Nyquist diagrams, the reported conductivity values are total conductivities.

3. Results

3.1. Thermal behavior

Fig. 2 presents the dilatometric curves on a mixture of starting materials (La_2O_3, SiO_2, $BaCO_3$) pressed pellets and Table 1 presents the final densities of the sintered samples. We notice that we have a low densification of all compounds at 1500 °C: this temperature is therefore suitable for the calcination of the mixtures of starting materials. The compounds with $x \leq 1$ have a classical sintering behavior between 1400 and 1600 °C. The two compositions $La_8Ba_2Si_6O_{26}$ and $La_{8.5}Ba_{1.5}Si_6O_{26.25}$ have an unusual behavior. The $La_{8.5}Ba_{1.5}Si_6O_{26.25}$ composition presents a low final shrinkage. The $La_8Ba_2Si_6O_{26}$ composition presents a rapid sintering rate above 1400 °C with a very high total shrinkage. We cannot explain the difficulty to sinter the $La_{8.5}Ba_{1.5}Si_6O_{26.25}$ compound. The apatite compound $La_8Ba_2(SiO_4)_6O_2$ sintering is activated at lower temperature than the other compounds. Secondary phase $Ba(SiO_2)_3$ (not observed on X-ray diffraction patterns) is likely to appear due to the existence of an eutectic between BaO and SiO_2

Table 1
Materials densities

Compound	Theoretical density	% of theoretical density
$La_8Ba_2Si_6O_{26}$	5.40	96.4
$La_{8.5}Ba_{1.5}Si_6O_{26.25}$	5.45	85.6
$La_9Ba_1Si_6O_{26.5}$	5.51	96.9
$La_{9.25}Ba_{0.75}Si_6O_{26.62}$	5.55	96.9
$La_{9.5}Ba_{0.5}Si_6O_{26.75}$	5.57	96.2
$La_{9.75}Ba_{0.25}Si_6O_{26.87}$	5.59	95.8
$La_{9.33}Si_6O_{26}$	5.31	97.9

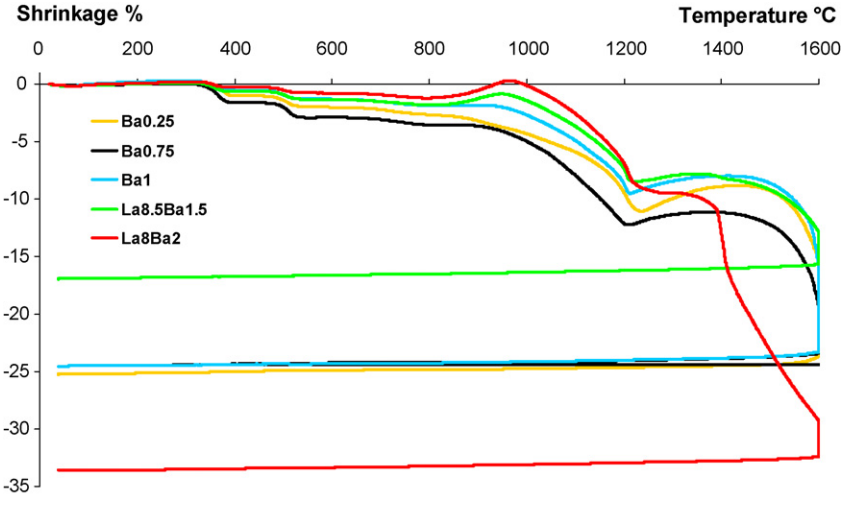

Fig. 2. Dilatometric curves of starting materials.

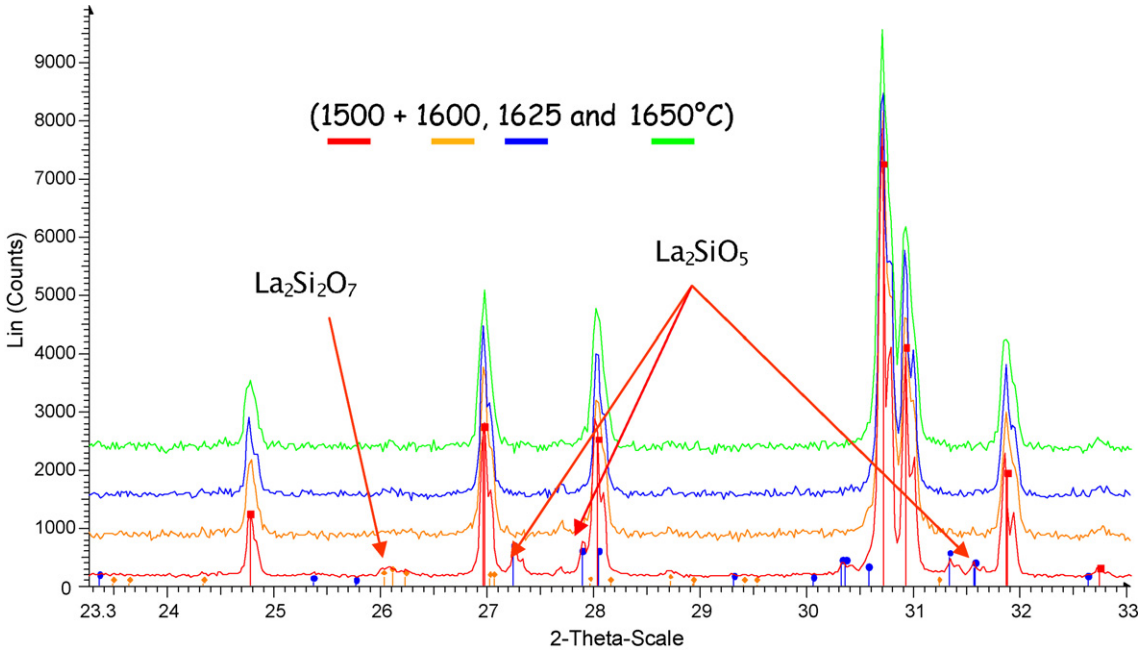

Fig. 3. XRD Patterns on $La_{9.33}(SiO_4)_6O_2$ for different calcination temperatures.

at the molar ratio $BaO/SiO_2 = 1/3$ (the apatite composition $La_8Ba_2(SiO_4)_6O_2$ has a Ba/Si molar ratio of 1/3). For the other Ba doped apatite compositions, the sintering temperature decreases lightly with the doping level.

3.2. XRD study

We will first consider our composition of reference $La_{9.33}Si_6O_{26}$. According to the La_2O_3/SiO_2 phase diagram[18],

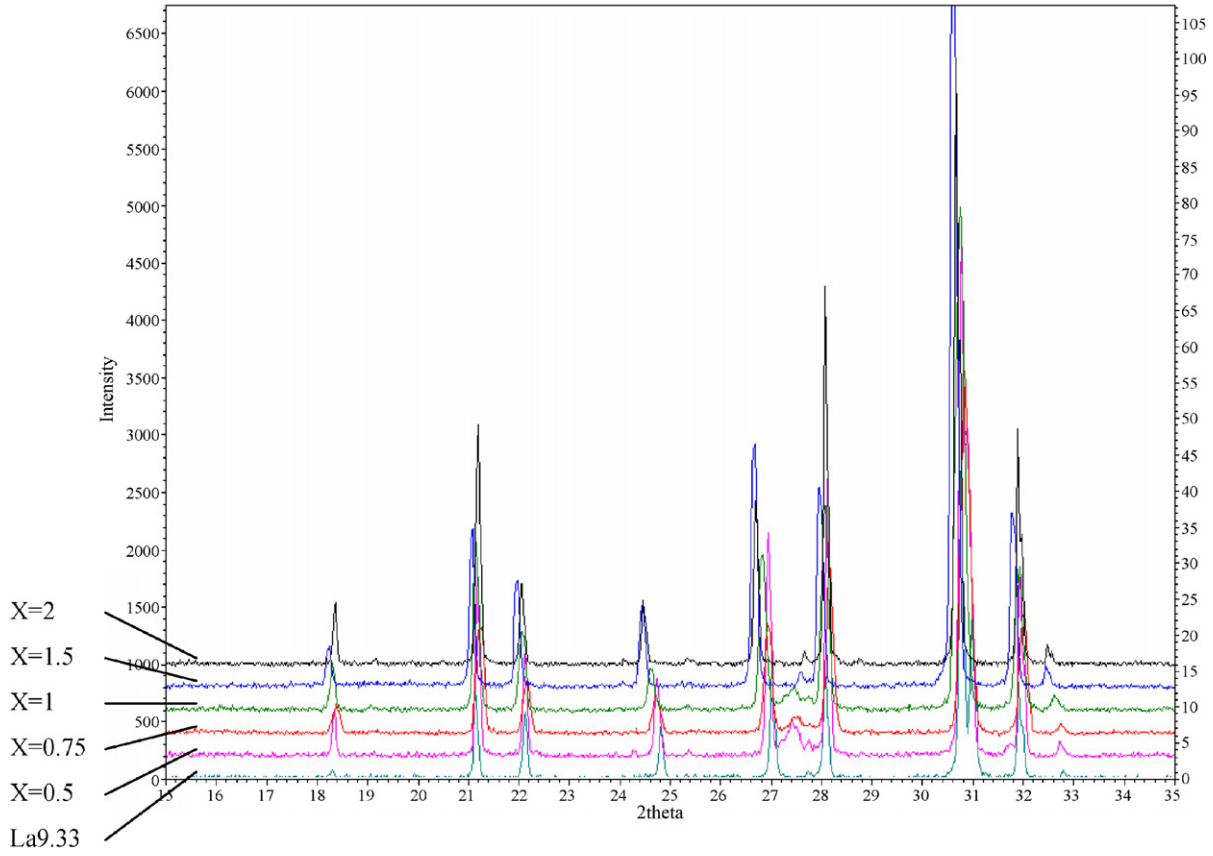

Fig. 4. XRD patterns on $La_{10-x}Ba_x(SiO_4)_6O_{3-x/2}$ apatite pellets for a 1625 °C calcination temperature.

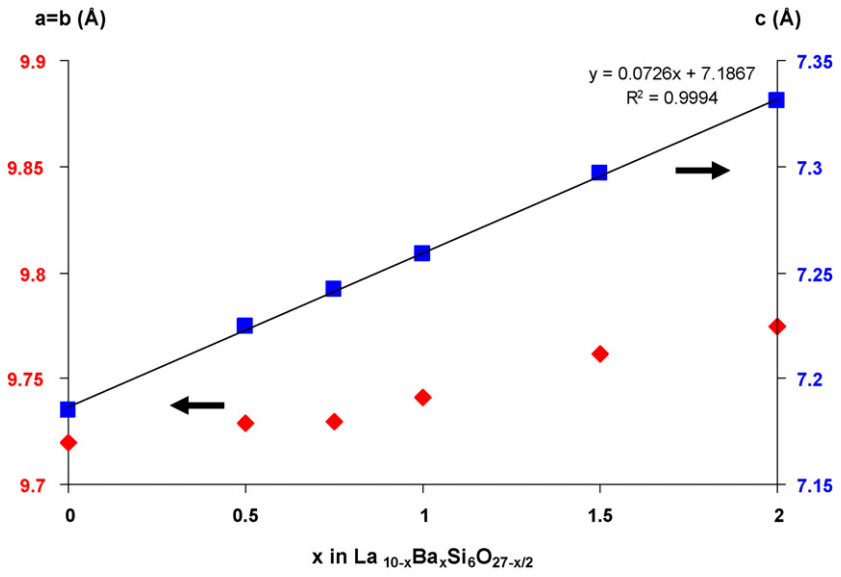

Fig. 5. Evolution of the lattice parameters versus the barium content.

the apatite is not the most thermodynamically stable phase at 1500 °C: La_2SiO_5 and $La_2Si_2O_7$ phases are more stable than apatite below 1600 °C. If kinetic allows the apatite formation at this temperature, a temperature higher than 1600 °C is required to obtain pure materials. Fig. 3 presents the X-ray diffraction patterns obtained at different firing temperatures (1500, 1600, 1625 and 1650 °C). The secondary phases (La_2SiO_5 and $La_2Si_2O_7$) disappear when the firing temperature increases. Sintering at 1625 °C for 30 min gave pure apatite powders. This sintering temperature was applied to the Ba doped apatite compounds. Fig. 4 compares X-ray diffraction patterns of Ba doped $La_{10-x}Ba_x(SiO_4)_6O_{3-x/2}$ $(0.5 \leq x \leq 2)$ and $La_{9.33}(SiO_4)_6O_2$ apatites. No diffraction peak that could be assigned to a secondary phase was observed. The "peak" observed between 27.2° and 27.95° (2θ) is due to the massive form of the sample. The evolution of the lattice parameters of the apatite phase versus Ba content are shown in Fig. 5. We see that the Vegard's law is respected for the "c" parameter (tunnel axis) but not for the "$a = b$" parameter at low Ba contents. The cell presents an anisotropic growing along the "c" axis. This phenomenon is explained by the substitution of Ba for La. Ba is larger than La in coordination 7 or 9. We can assume that the Ba substitutes for La on the 4f site (coordination 9) first. As this site is located between two ionic planes, its expansion has more influence on the distance between the ionic planes ("c" axis) than

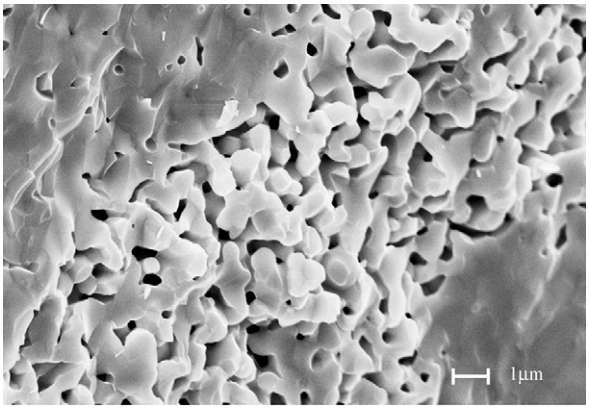

Fig. 7. SEM observation of $La_{8.5}Ba_{1.5}(SiO_4)_6O_{2.25}$.

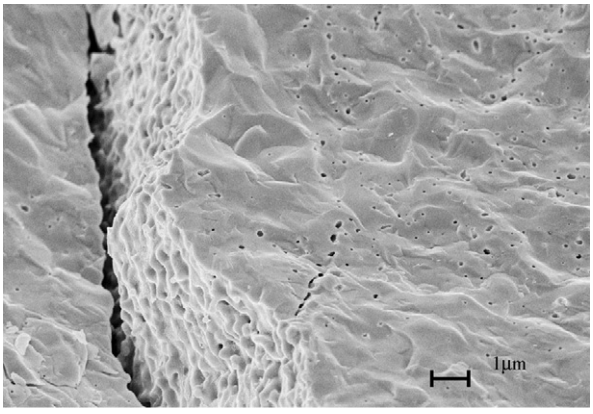

Fig. 6. Representative SEM observation of an apatite sample.

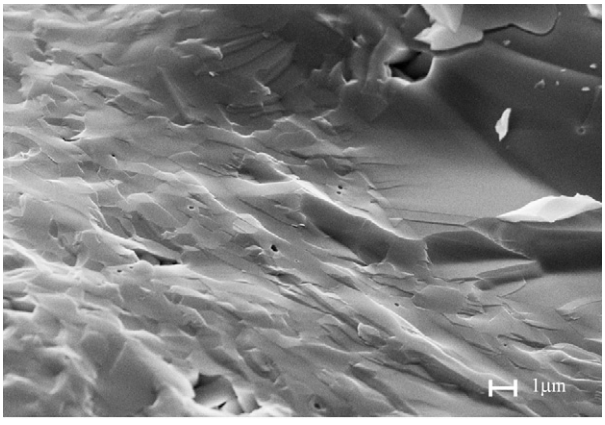

Fig. 8. SEM observation of $La_8Ba_2(SiO_4)_6O_2$.

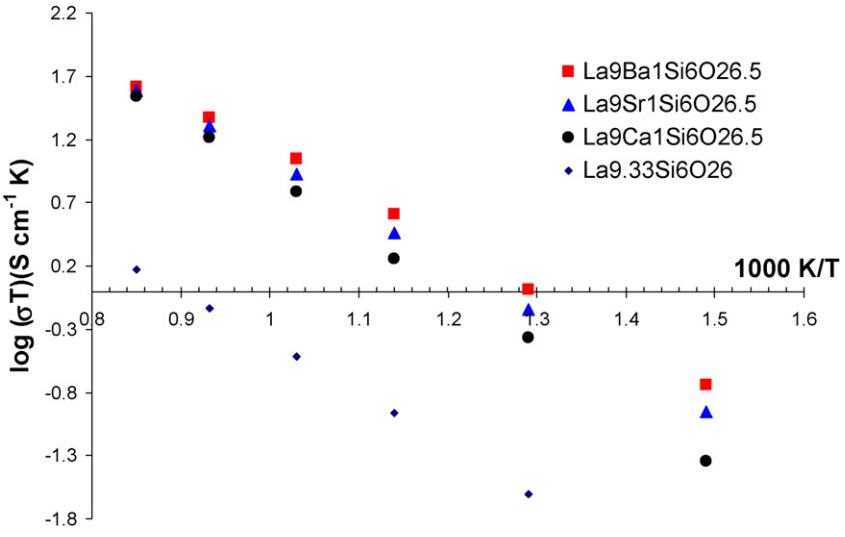

Fig. 9. Arrhenius diagram/comparison with Ca and Sr doped apatites and undoped apatite.

on the planes themselves (*a* and *b* axes). When the Ba content becomes significant ($x \geq 1$), we also observe an "$a = b$" axis expansion due to the substitution of Ba for La on the 6h site.

3.3. Microstructure

Microstructural SEM observations were performed on all fractured samples. Fig. 6 is a representative microstructure of a barium doped apatite. We observe a homogeneous material. The $La_{8.5}Ba_{0.5}Si_6O_{26.25}$ SEM observation in Fig. 7 shows a heterogeneous material with at once densified and very porous areas. In the case of $La_8Ba_2(SiO_4)_6O_2$ in Fig. 8, the liquid phase sintering is demonstrated by the SEM observation which shows a heterogeneous material with small grain and very large grain areas.

3.4. Ionic conductivities

Due to their heterogeneous microstructure, it was not possible to characterize the electrochemical properties of the apatite compounds $La_{8.5}Ba_{1.5}(SiO_4)_6O_{2.25}$ and $La_8Ba_2(SiO_4)_6O_2$. Both compounds may indeed need a refined process in order to optimize the microstructures of the pellets. The apatite compound $La_9Ba_1(SiO_4)_6O_{2.5}$, which is finally the best material in terms of phase purity and density, was studied by impedance spectroscopy. We assume the resolution of bulk and grain boundary semicircles at low temperatures (300 and 400 °C). At middle temperature (500 and 600 °C) only a partial grain boundary contribution is observed and at high temperatures (700 to 900 °C) only the electrode response. Fig. 9 presents the Arrhenius diagrams of the $La_{9.33}(SiO_4)_6O_2$ and $La_9Ba_1(SiO_4)_6O_{2.5}$ compounds, and compares them with some equivalent strontium and calcium doped $La_9Sr_1(SiO_4)_6O_{2.5}$ and $La_9Ca_1(SiO_4)_6O_{2.5}$ compounds. The conductivity values at 700 °C and the activation energies are reported in Table 2. We notice first the low conductivity of the undoped apatite and significant increase of conductivity with a doping on the La site, whatever the dopant nature. This figure also highlights the influence of the dopant size on the apatite conductivity. The best conductivity and the lowest activation energy are observed for the Ba doping (11.4 mS cm^{-1} at 700 °C and 0.75 eV), following the Sr and the Ca doped apatites.

Table 2
Conductivities and activation energies of doped apatites and YSZ

Slope	Compound	E_a (kJ/mol)	E_a (eV)	Conductivities at 700 °C (mS cm^{-1})
−3.84	$La_9Ba_1Si_6O_{26.5}$	73	0.75	11.4
−4.01	$La_9Sr_1Si_6O_{26.5}$ [13]	76	0.79	8.7
−4.50	$La_9Ca_1Si_6O_{26.5}$ [13]	86	0.88	6.3
−4.19	YSZ [19]	80	0.82	22.8
−4.53	$La_{9.33}Si_6O_{26}$	87	0.89	0.3

4. Conclusion

Ba doped and undoped apatites were synthesized with a high purity level, using a classical solid state reaction elaboration process. Anyway it seems that a high temperature treatment (>1600 °C) is required in order to purify the apatite phase. XRD shows total insertion of the barium in the apatite lattice. Dilatometric studies and SEM observations reveal a special behavior of the $La_{8.5}Ba_{1.5}(SiO_4)_6O_{2.25}$ and $La_8Ba_2(SiO_4)_6O_2$ compounds, which may be explained for $La_8Ba_2(SiO_4)_6O_2$ by the existence of an eutectic in the BaO/SiO_2 phase diagram. The study of the ternary diagram ($La_2O_3/SiO_2/BaO$) may be able to solve the problems observed at high doping levels ($x > 1$). The conductivity study shows that the barium doped apatite has the best conductivity and the lowest activation energy compared to some equivalent strontium or calcium doped apatites.

References

1. Nakayama, S., Sakamoto, M., Higuchi, M., Kodaira, K., Sato, M., Kakita, S., Suzuki, T. and Itoh, K., Oxide ionic conductivity of apatite type $Nd_{9.33}(SiO_4)_6O_2$ single crystal. *J. Eur. Ceram. Soc.*, 1999, **19**, 507–510.
2. Nakayama, S., Sakamoto, M., Higuchi, M. and Kodaira, K., Ionic conductivities of apatite type $Nd_x(SiO_4)_6O_{1.5x-12}$ ($x = 9.20$ and 9.33) single crystals. *J. Mater. Sci. Lett.*, 2000, **19**, 91–93.
3. Nakayama, S., Kageyama, T., Aono, H. and Sadaoka, Y., Ionic Conductivity of Lanthanoid Silicates, $Ln_{10}(SiO_4)_6O_3$ (Ln = La, Nd, Sm, Gd, Dy, Y, Er and Yb). *J. Mater. Chem.*, 1995, **5**(11), 1801–1805.
4. Nakayama, S. and Higuchi, M., Electrical properties of apatite-type oxide ionic conductors $RE_{9.33}(SiO_4)_6O_2$ (RE = Pr, Nd and Sm) single crystals. *J. Mater. Sci. Lett.*, 2001, **20**, 913–915.
5. Abram, E. J., Sinclair, D. C. and West, A. R., A novel enhancement of ionic conductivity in the cation-deficient apatite $La_{9.33}(SiO_4)_6O_2$. *J. Mater. Chem.*, 2001, **11**, 1978–1979.
6. Leon-Reina, L., Cabeza, E. R. L. A., Martinez-Lara, M., Bruque, S. and Aranda, M. A. G., Interstitial oxygen conduction in lanthanum oxy-apatite electrolytes. *J. Mater. Chem.*, 2004, **14**, 1142–1149.
7. Sansom, J. E. H. and Slater, P. R., The Synthesis and Conductivities of the New Apatite-Type Phases $La_{10-x}Si_{6-y}Ga_yO_{26+z}$ and Related Systems. *Solid State Ionics*, 2004, **167**, 17–22.
8. Felsche, J., Rare earth silicates with the apatite structure. *J. Solid State Chem.*, 1972, **5**, 266–275.
9. Samson, J. E. H., Tolchard, J. R., Slater, P. R. and Islam, M. S., Synthesis and structural characterisation of the apatite-type phases $La_{10-x}Si_6O_{26+z}$ doped with Ga. *Solid State Ionics*, 2004 17–22 Feb., **167** (1–2).
10. Sansom, J. E. H., Richings, D. and Slater, P. R., A powder neutron diffraction study of the oxide-ion-conducting apatite-type phases, $La_{9.33}Si_6O_{26}$ and $La_8Sr_2Si_6O_{26}$. *Solid State Ionics*, 2001, **139**, 205–210.
11. Slater, P. R. and Samson, J. E. H., The synthesis and characterisation of new apatite-type oxide ion conductors. *Solid State Phenom.*, 2003, **90–91**, 195–200.
12. Najib, A., Sansom, J. E. H., Tolchard, J. R., Slater, P. R. and Islam, M. S., Doping strategies to optimize the oxide ion conductivity in apatite-type ionic conductors. *Dalton Trans.*, 2004, 3106–3109.
13. Savignat, S. B., Lima, A., Barthet, C. and Henry, A., In *Proceedings of the internationnal Symposium SOFC, vol. VIII*, 2003, pp. 372–378.
14. Knizek, K., *KDif*, K. Software, Editor. 2005: Praha.
15. Petricek, V. and Dusek, M., *Jana2000*. 2004: Praha.
16. Derek, J., *Zplot*, I. Scribner Associates, Editor. 1999.
17. Derek, J., *Zview*, I. Scribner Associates, Editor. 2005.
18. Toporov, N. A. and Bondar, I. A., Silicates of the rare earth elements. IV. New silicates in the lanthanum oxide-silica system. *Uch. Zap. Kazan. Gos. Univ.*, 1961, **5**, 739–744.
19. Kharton, V. V., Marques, F. M. B. and Atkinson, A., Transport properties of solid oxide electrolyte ceramics: a brief review. *Solid State Ionics*, 2004, **174**(1–4), 135–149.